International Journal of Thermodynamics (IJoT)
ISSN 1301-9724 / e-ISSN 2146-1511
https://dergipark.org.tr/en/pub/ijot

Vol. 26 (No. 4), pp. 019-030, 2023
doi: 10.5541/ijot.1248571
Published online: December 1, 2023

Research Article

New Thermodynamic Equation of State for Refrigerant HFO-1243zf

[1]*I. M. Astina, [2]H. I. Alfisahri

[1,2] Faculty of Mechanical and Aerospace Engineering, Institut Teknologi Bandung, West Java, Indonesia
E-mails: [1]*astina@itb.ac.id, [2]hilmyilham67@gmail.com

Received 8 February 2023, Revised 26 April 2023, Accepted 20 May 2023

Abstract

R-1243zf is a new refrigerant that could replace R-134a. Its thermodynamic properties represented in the equation of state (EOS) play an essential role in analyzing and designing thermal systems. The EOS exists without including caloric property data due to unavailable data during the development time. New EOS was developed explicitly in Helmholtz free energy and optimized to represent the experimental data accurately and maintain thermodynamic consistency. The optimization process undergoes using a genetic algorithm and weighted-least squares regression. The experimental data used in the optimization have a range of 233–430 K and 0.106–34.6 MPa and were validated from the extrapolation and consistency to confirm the reliability. The average absolute deviation from the data is 0.48% for the ideal gas isobaric specific heat, 1.7% for the isochoric specific heat, 0.33% for the speed of sound, 0.22% for the liquid density in single-phase, 0.49% for the vapor density in single-phase, 0.96% for the vapor pressure, 2.2% for the saturated liquid density, and 3.2% for the saturated vapor density. The EOS has a reasonable extrapolation behavior from the triple point up to 700 K and 100 MPa.

Keywords: *Modeling; thermodynamic properties; equation of state; HFO refrigerant; R-1243zf.*

1. Introduction

The development of research in the refrigerant is still undergoing in response to the issues of ozone depletion and global warming, as well as the efforts to establish efficient thermal systems. The 2016 Kigali Amendment to the Montreal Protocol is an international agreement to phase down the consumption and production of hydrofluorocarbons (HFCs) [1]. Refrigerant tetrafluoro-ethane (R-134a) is widely spread and installed in refrigeration and air conditioning systems, but it has very high global warming effect. Therefore, it is necessary to look for solutions to replace these refrigerants in existing machines and develop new and environmentally friendly systems. Refrigerant 3,3,3-trifluoropropene (R-1243zf) has majorly similar properties to R-134a, so it is attractive as an alternative refrigerant and is the same potential substitution as R-1234yf and trans-1,3,3,3-tetrafluoropropene (R-1234ze(E)). Emissions of R-1243zf have no impact on ozone depletion but have a global warming potential (GWP) of less than one [2], as well as its mildly flammable in group A2L [3]. R-134a is widely and commonly used in organic Rankine, residential refrigeration, and vehicle cooling systems [4]. Recently, many publications regarding the experimental data and measurement of various thermodynamic properties of R-1243zf are available and described in more detail in Section 2. This fact indicates that the R-1243zf is widely still considered to be applied.

Thermodynamic properties, which play an essential role in the analysis and design of thermal systems, may be expressed in terms of Helmholtz free energy. The state-of-the-art equation of state (EOS) for R-1243zf was introduced by Akasaka [5] and Akasaka and Lemmon [6]. These equations are multiparameter EOS used to represent a pure fluid or expanded to its mixture. Both EOS were developed without caloric data such as isochoric and isobaric specific heats, so inquiring about the accuracy of these properties. Subsequently, new caloric data such as isochoric specific heat, ideal gas isobaric specific heat, and speed of sound followed the existing EOSs. The new caloric data include data from Sheng et al. [7] and Chen et al. [8]. The accuracy of data on the caloric properties directly relates to enthalpy and entropy used in the analysis and design of thermal energy systems. The new EOS for R-1243zf needs the latest data fitted. Therefore, this article presents a new EOS, considering the latest data, thermodynamic consistency, and comprehensive assessment in modeling.

2. Survey and Available Data

Hydrofluoroolefin (HFO) is a fourth-generation refrigerant and alternative to HFCs [4]. The usage of HFCs reduces due to their high GWP effect. HFOs have a C=C double bond structure, free of chlorine, and have a short atmospheric lifetime. In addition, HFOs, which are environmentally friendly and much like HFCs, are expected to be suitable as substitutes. One of the HFOs with great potential is R-1243zf. This refrigerant, herewith the R-1234yf and R-1234ze(E), has similar thermodynamic properties to HFC-134a. R-1243zf is a good choice for the substitute because it has the most similar characteristics to R-134a compared to the others and has a better coefficient of performance in several models.

A critical pressure and temperature were taken from Higashi and Sakoda [9]. The critical density and the triple point temperature derived from the EOS of Akasaka and

*Corresponding Author

Lemmon [6] were due to unavailable experimental data. The critical temperature and density function as reduction parameters for temperature and density, respectively. The critical temperature (T_c) and pressure (p_c) are 376.93 K and 3.518 MPa [9], respectively. The critical density (ρ_c) is 413.02 kg·m^{-3} [6], and triple point temperature (T_{tp}) is 220 K [6]. Additionally, the universal gas constant ($\bar{R}$) used is 8.314462618 J·mol^{-1}·K^{-1} [10], and the molecular mass (M) is 96.05113 kg·kmol^{-1} [7].

The PVT data, either at saturation or in a single phase, are required to develop the EOS. The saturation data from the triple point to the critical point are essential input data on the development. The PVT data in the single phase covers the liquid and gas phases, including the supercritical region. Additionally, caloric properties significantly improve the accuracy of EOS to represent specific heat, enthalpy, and entropy. The data required are in a wide range for the development of the EOS. Furthermore, the collected data are available in Table 1.

Table 1. Available experimental data for R-1243zf.

No	Prop.	Source	Points	Range	
				MPa	K
1	p_s	Raabe and Marginn [11]	10	-	263–353
2	p_s	Brown et al. [12]	83	-	233–372
3	p_s	Higashi et al. [13]	20	-	310–376
4	p_s	Yin et al. [14]	26	-	253–376
5	p_s	Yang et al. [15]	17	-	273–353
6	ρ'	Raabe and Marginn [11]	10	-	263–353
7	ρ'	Higashi and Sakoda [9]	6	-	366–376
8	ρ''	Raabe and Marginn [11]	10	-	263–353
9	ρ''	Higashi and Sakoda [9]	7	-	366–376
10	PVT	Di Nicola et al. [16]	410	1.11–26.9	278–368
11	PVT	Higashi and Sakoda [9]	75	0.235–32.5	328–430
12	PVT	Yin et al. [14]	128	0.106–2.88	253–368
13	c_v	Sheng et al. [7]	64	1.58–10.21	299–351
14	c_p^0	Chen et al. [8]	11	-	313–363
15	w	Chen et al. [8]	92	0.170–1.98	313–363

The data at the saturation condition are used to develop ancillary equations and the residual part of the EOS. For vapor pressure, data from Higashi et al. [13], Raabe and Marginn [11], and Brown et al. [17] is also used in the equations of Akasaka and Lemmon [6]. Yin et al. [14] and Yang et al. [12] data are the most recent data. For density, no new data is available yet. The distribution of PVT experimental data is shown in Figure 1. The newly published data set is that of Yin et al. [14]. The data of Nicola et al. [16] has a broader range than the data of Higashi and Sakoda [9].

The caloric property data are not as abundant as other data. There are two resources, one for isochoric-specific heat and the other for speed of sound. This data distribution is shown in Figure 2. Sheng et al. [7] reported the data set for isochoric specific heat. As same as the specific-heat data, the speed-of-sound data was reported by Chen et al. [8]. Both data are newer than the existing EOS of Akasaka and Lemmon [6]. These data are inputted into the optimization process of the residual part. This data set plays an essential role in the development and assessment and is closely related to energy analysis. The distribution of the data is shown in Figure 2. These data are less than the PVT data, and the temperature and pressure ranges are still narrow.

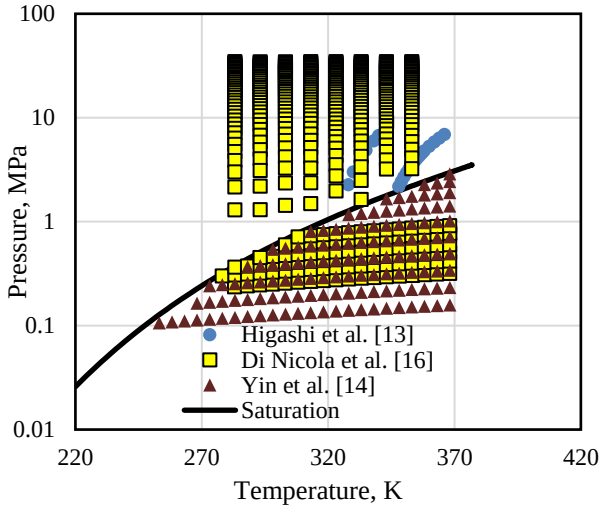

Figure 1. Data distribution of PVT properties.

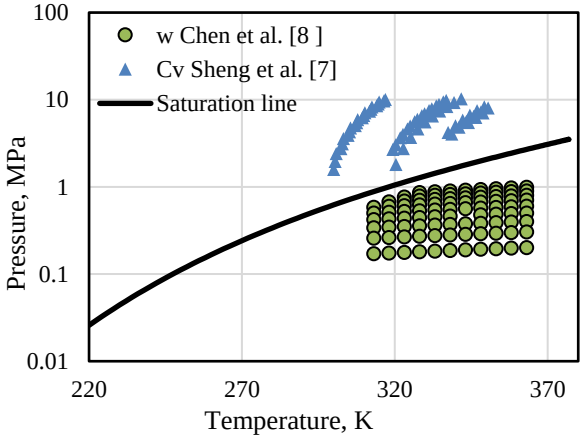

Figure 2. Data distribution of caloric properties.

The ideal gas isobaric heat data is analytical data derived from experimental data for the speed of sound. This data is used in the process of optimizing the ideal part of EOS. When the Akasaka and Lemmon equations [6] were developed, data for the isobaric-specific heat of an ideal gas were not yet available, so the data from analytical modeling based on the molecule's shape using the Joback-Reid method [17] was used. Now available data from the experimental results can be used, namely data from Chen et al. [8]. The amount of data generated is very limited, but its role is essential to verify and improve the quality of the previous equation.

The second and third virial coefficient data are involved in the equational optimization process of the residual part of EOS. Publication of experimental data on pressure, temperature, and density usually includes the second and third virial coefficient equations modeled from the experimental data, for example, the publication of Yin et al. [14]. Chen et al. [8] reported eleven data points for the second and third virial coefficients. Data from Yin et al. [14]

are valid in the range of 253–368 K because the measurement is in that range.

3. Modeling and Formulation

Mathematical modeling of thermodynamic properties is very complex because the relationship between one property and another is interrelated for a state. This complexity arises when one wishes to construct EOS in which one mathematical model can account for all the thermodynamic properties at a known state. Modeling for this case in the field of thermodynamic properties is referred to as multi-property modeling. The explanation of this multiparameter EOS modeling was given in detail by Span [18]. In mathematical thermodynamics, the relationship between fluid properties with the help of thermodynamic laws and definitions can be processed to obtain the relationship between these properties. Table 2 represents thermodynamic property relation respect to EOS with basis of Helmholtz free energy. EOS is fitted to input data as regression process to get an accurate one.

Optimization of the equation's structure is a part of the process of finding accurate and reliable equations. One step of the optimization procedure in this work uses a genetic algorithm. Genetic algorithms find the functional form of the equation, which is usually a power or exponential number that is hard to regress. The genetic algorithm optimization method combines random solutions and evolutionary processes. Optimization using the random solution method could always produce the best solution but requires an evaluation process for all combinations that could take very long time for complex cases such as the modeling of thermodynamic equations. Genetic algorithms imitate evolution based on natural selection, especially on chromosomes or genetics. Through this approach, the optimization process becomes focused on a convergent value approaching the best solution with fewer evaluation processes than the random solution method so that the optimization process becomes much faster. Fitness is the sum of the least squares objective function with its weighting factor. For multi-property optimization, the resulting fitness is the sum of the regression results of all the properties included in the optimization.

The process of developing for the thermodynamic model uses a genetic algorithm to find non-linear terms and uses least squares linear regression to obtain linear coefficients. The developed models consist of EOS and ancillary equations for vapor pressure, saturated liquid, and saturated vapor densities. Adhering to the concept of the different properties between ideal gas and real-fluid properties, the EOS is divided into two parts: ideal and residual parts. The regression model presented in Eq. (1) includes the mathematical relation in Table 2. Variable *W* in the equation is the weighting factor, y_{data} is the measured data (property input), and y_{cal} is the property calculated based on density and temperature input for a case of developing EOS and based on temperature for case developing the ancillary equations. The y_{data} is filled with values from the left side; the y_{cal} is from the right side in the mathematical equations.

$$\chi = \sum_{i=1}^{n} W_i (y_{data} - y_{cal})^2 \quad (1)$$

The properties included in modeling depend on available input data. However, pressure-volume-density and caloric property data must be included, aside from Maxwell's relation of vapor pressure and virial coefficients. The sum of least square (χ) is minimized in regression processes to get accurate models.

Table 2. Thermodynamic relations respect to EOS.

Properties	Mathematical relations
Helmholtz free energy	$\alpha = \frac{A}{RT} = \alpha^o + \alpha^r$
Ideal gas isobaric specific heat	$\frac{c_p^0}{R} = 1 - \tau^2 \alpha_{\tau\tau}^0 = 1 + \frac{c_v^0(\tau)}{R}$
Pressure	$\frac{p(\delta,\tau)}{\rho RT} = 1 + \delta \alpha_\delta^r$
Vapor pressure	$\frac{p_s(\delta',\delta'',\tau_s)}{RT_s} = \frac{\rho'\rho''}{\rho' - \rho''}\left(\ln\left(\frac{\delta'}{\delta''}\right) + \alpha^{r\prime} - \alpha^{r\prime\prime}\right)$
Isobaric specific heat	$\frac{c_p(\delta,\tau)}{R} = \frac{c_v(\delta,\tau)}{R} + \frac{(1+\delta\alpha_\delta^r - \delta\tau\alpha_{\delta\tau}^r)^2}{(1+2\delta\alpha_\delta^r + \delta^2\alpha_{\delta\delta}^r)}$
Isochoric specific heat	$c_v(\delta,\tau)/R = -\tau^2(\alpha_{\tau\tau}^0 + \alpha_{\tau\tau}^r)$
Saturated liquid specific heat	$\frac{c_s{}'(\delta',\delta'',\tau_s)}{R} = \frac{c_v(\delta',\tau_s)}{R} + \frac{(1+\delta'\alpha_\delta^{r\prime} - \delta'\tau_s\alpha_{\delta\tau}^{r\prime})}{(1+2\delta'\alpha_\delta^{r\prime} + \delta'^2\alpha_{\delta\delta}^{r\prime})} \times \left\{1 + \delta'\alpha_\delta^{r\prime} - \delta'\tau_s\alpha_{\delta\tau}^{r\prime} - \frac{1}{R\rho_c\delta'}\frac{dp_s(\delta',\delta'',\tau_s)}{dT}\right\}$
Saturated vapor specific heat	$\frac{c_s{}''(\delta',\delta'',\tau_s)}{R} = \frac{c_v(\delta'',\tau_s)}{R} + \frac{(1+\delta''\alpha_\delta^{r\prime} - \delta''\tau_s\alpha_{\delta\tau}^{r\prime\prime})}{(1+2\delta''\alpha_\delta^{r\prime\prime} + \delta''^2\alpha_{\delta\delta}^{r\prime\prime})} \times \left\{1 + \delta''\alpha_\delta^{r\prime\prime} - \delta''\tau_s\alpha_{\delta\tau}^{r\prime\prime} - \frac{1}{R\rho_c\delta''}\frac{dp_s(\delta',\delta'',\tau_s)}{dT}\right\}$
Speed of Sound	$\frac{w^2(\delta,\tau)M}{RT} = 1 + 2\delta\alpha_\delta^r + \delta^2\alpha_{\delta\delta}^r + \frac{(1+\delta\alpha_\delta^r - \delta\tau\alpha_{\delta\tau}^r)^2}{c_v(\delta,\tau)/R}$
Enthalpy	$\frac{h(\delta,\tau)}{RT} = \tau(\alpha_\tau^0 + \alpha_\tau^r) + 1 + \delta\alpha_\delta^r$
Entropy	$\frac{s(\delta,\tau)}{R} = \tau(\alpha_\tau^0 + \alpha_\tau^r) - (\alpha^0 + \alpha^r)$
Internal energy	$\frac{u(\delta,\tau)}{RT} = \tau(\alpha_\tau^0 + \alpha_\tau^r)$
Third virial coefficient	$B(\tau)\rho_c = \lim_{\delta\to 0}\alpha_\delta^r$
Second virial coefficient	$C(\tau)\rho_c^2 = \lim_{\delta\to 0}\alpha_{\delta\delta}^r$
$\delta = \frac{\rho}{\rho_c}$, $\tau = \frac{T_c}{T}$, $R = \frac{\bar{R}}{M}$, $A = u - Ts$, $\alpha_\delta = \left(\frac{\partial\alpha}{\partial\delta}\right)_\tau$, $\alpha_\tau = \left(\frac{\partial\alpha}{\partial\tau}\right)_\delta$, $\alpha_{\delta\delta} = \left(\frac{\partial^2\alpha}{\partial\delta^2}\right)_\tau$, $\alpha_{\tau\tau} = \left(\frac{\partial^2\alpha}{\partial\tau^2}\right)_\delta$, $\alpha_{\delta\tau} = \left(\frac{\partial^2\alpha}{\partial\delta\partial\tau}\right)$	

Both ancillary equations and EOS must be able to provide accurate calculation results. The ancillary equations play an essential role in preparing input data for developing

the EOS and initial guess for the iteration process conducted in calculating thermodynamic properties when one or more unknown properties are the independent variables.

The most complex EOS formulation today is the IAPWS 1995 equation for ordinary water by Wagner and Pruß [19]. For EOS based on the Helmholtz free energy, regardless of the complexity of the formulation given, derivation of the other thermodynamic properties from the Helmholtz free energy still has the same fundamental mathematical relationship so that the previous mathematical relation can be applied to calculate the properties. The modeling procedure and program code used in this study were used for refrigerants of HFC, hydrocarbon, HFO, and hydrochlorofluoroolefin (HCFO). Our recent article reported their implementation for HFO [20] dan HCFO [21]. More detailed optimization procedures used can be found in previous work [22].

4. Thermodynamic Property Model

The thermodynamic property models as results of this study consist of ancillary equations for vapor pressure, saturated liquid density, and saturated vapor density as well as the EOS.

4.1 Ancillary Equation

The optimization process of ancillary equations uses a genetic algorithm. The ancillary equation for the density of saturated vapor is expressed on a logarithmic basis, while the equation for the saturated liquid density has a linear basis. The saturated vapor pressure correlates with the temperature (T) with four terms as given in Eq. (2). Critical pressure (p_c) and critical temperature (T_c) are inside for getting dimensionless relation. The exponents of the equation terms on the right side are the results of optimization with a genetic algorithm. Variable E is the coefficients obtained from the optimization process, which are E_1 = -7.3416, E_2 = -3.1588, E_3 = -3.1012, and E_4 = -4.1381. The sum of the terms used in this equation equals the ancillary equation used by Akasaka and Lemmon [6]. The term number is sufficient to represent the properties properly and is small enough to run a quick calculation process.

$$\ln\left(\frac{p}{p_c}\right) = \frac{T_c}{T}\left(E_1\left[1-\frac{T_c}{T}\right] + E_2\left[1-\frac{T_c}{T}\right]^{1.6} + E_3\left[1-\frac{T_c}{T}\right]^{2} + E_4\left[1-\frac{T_c}{T}\right]^{5}\right) \quad (2)$$

The next two ancillary equations for saturated liquid density (ρ') and saturated vapor density (ρ''), respectively, are written in Eqs. (3) and (4). Both equations are represented in dimensionless with dividing with critical density (ρ_c) and critical temperature. The equations have four terms. Variables F and G are coefficients as optimization processes in their development. The coefficients obtained are F_1 = 0.018161, F_2 = -0.53941, F_3 = 2.5054, F_4 = 0.75331, G_1 = 0.89105, G_2 = -3.3802, G_3 = -7.8192, and G_4 = -31.145.

$$\frac{\rho'}{\rho_c} = 1 + F_1\left[1-\frac{T}{T_c}\right]^{0.1} + F_2\left[1-\frac{T}{T_c}\right]^{0.2} + F_3\left[1-\frac{T}{T_c}\right]^{0.3} + F_4\left[1-\frac{T}{T_c}\right]^{0.9} \quad (3)$$

$$\ln\left(\frac{\rho''}{\rho_c}-1\right) = G_1\left[1-\frac{T}{T_c}\right]^{0.2} + G_2\left[1-\frac{T}{T_c}\right]^{0.3} + G_3\left[1-\frac{T}{T_c}\right]^{1.2} + G_4\left[1-\frac{T}{T_c}\right]^{3.8} \quad (4)$$

The terms used are less than the term from the ancillary equations used by Akasaka and Lemmon [6]. The use of fewer terms makes the calculation process faster without sacrificing the accuracy of the equation. The ancillary equations for the densities of saturated liquid and saturated vapor to assist the optimization process of the EOS and as the initial iteration value in root calculation to find thermodynamic properties either in single-phase or two-phase for the case of known properties excluding temperature or density.

4.2 New Helmholtz Equation of Sate

The new EOS (α) consists of two parts: the ideal part (α^o) and the residual part (α^r) and the relation is $\alpha = \alpha^o + \alpha^r$. The ideal part is obtained by integrating the ideal-gas isobaric specific heat equation at a reference state. The ideal gas isobaric heat equation should be obtained first as the final result in Eq. (5). The equation has just two terms of the Einstein-Planck functional form. In this short relation, the equation can represent satisfied accuracy. The residual part must be prepared prior to complete the ideal part with its two integral constant values because of the reference state selected for the EOS is not in the ideal gas state. Finally, the new EOS is fitted to a reference state of the International Institute of Refrigeration. The final result of the ideal part is written in Eq. (6) with the numerical coefficients and constants in Table 3.

$$\frac{c_p^o(\tau)}{R} = \sum_{i=1}^{2} N_i^o \tau^2 b_i^2 \frac{\exp(-b_i\,\tau)}{\left(1-\exp(-b_i\,\tau)\right)^2} \quad (5)$$

$$\alpha^o(\delta,\tau) = \ln\frac{\delta}{\tau} + \sum_{i=1}^{2} N_i^o \ln(1-\exp(-b_i\,\tau)) + \sum_{i=3}^{4} N_i^o\,\tau^{b_i} \quad (6)$$

Table 3. Numerical coefficients of the ideal gas.

i	b_i	N_i^o
1	1.5050	1.3863×10^1
2	5.5650	9.6280×10^0
3	0	-1.1263×10^1
4	1	9.4400×10^0

The residual part obtained from this work appears in Eq. (7). Table 4 represents the numerical coefficients and constants of the equation. The polynomial terms of the equation usually represent the thermodynamic properties of the vapor phase, while the exponential terms of the equation represent the properties of the liquid phase [23]. The terms for the density variable must be integer, while the terms for the temperature variable must be real numbers. The value of the *t* term of the temperature variable functions for modeling the critical region [23]. Outside the critical region, the term τ^{t_i} can cause very high fluctuations so that it must be damped with the others, namely δ^{d_i} in the vapor phase and $\exp\left[-\delta^{\theta_i}\right]$ in the liquid phase.

$$\alpha^r(\delta,\tau) = \sum_{i=1}^{6} N_i \delta^{d_i}\tau^{t_i} + \sum_{i=7}^{20} N_i \delta^{d_i}\tau^{t_i}\exp\left[-\delta^{\theta_i}\right] \quad (7)$$

The combination of genetic algorithms and weighted least square regression is applied in the optimization program to obtain EOS and ancillary equations. EOS results from this study of a general structure to accommodate polynomials, exponentials, and Gaussian-Bell terms. The nonlinear correlations for caloric properties are compensated via a

limited iterative regression in the process of the optimal residual structure to represent the input data in the modeling.

Table 4. Numerical coefficients of the residual part.

i	d_i	t_i	θ_i	N_i
1	1	0.425	-	1.2694572×10^{0}
2	4	0.45	-	2.9865027×10^{-2}
3	2	1.3	-	$-8.5288450 \times 10^{-2}$
4	1	1.325	-	-2.5317951×10^{0}
5	3	1.9	-	$-6.0204735 \times 10^{-2}$
6	4	2	-	1.6375506×10^{-2}
7	2	3.525	1	$-4.7744050 \times 10^{-1}$
8	2	2.125	1	6.0054790×10^{-1}
9	3	2.235	1	8.6505374×10^{-1}
10	2	4.625	1	2.6476831×10^{1}
11	2	7	1	$-2.9446209 \times 10^{-2}$
12	1	7.125	1	-1.0141306×10^{0}
13	1	7.25	1	9.3621188×10^{-1}
14	5	2	2	$-8.5592024 \times 10^{-2}$
15	4	4	2	-6.3548921×10^{2}
16	6	5.875	2	3.5316930×10^{-2}
17	7	5.75	2	$-1.7172415 \times 10^{-2}$
18	1	0	3	$-3.6957644 \times 10^{-2}$
19	7	4.5	3	$-1.1731380 \times 10^{-2}$
20	2	6.5	3	$-8.7493600 \times 10^{-2}$

Compared with Akasaka and Lemmon, the combination of stepwise linear regression and nonlinear least-square regression to obtain the final EOS. Even though there are differences in the process, there are similarities in modeling: optimization of the equation structure and linear coefficient of the equation, and all constraints cannot be included directly in the optimization process but evaluated after getting the best model. The method used in this study, even though it operates with many equation structure predictions, the optimization process can still be faster. The developed EOS consists of polynomial and exponential terms simpler than the EOS of Akasaka and Lemmon [6].

5. Assessments

The evaluation for properties in single-phase is divided into two parts: gas phase and liquid phase. It is divided due to significantly different characteristics of the data in the gas phase and liquid phase, so the evaluation needs to be done separately. Experimental data of thermodynamic properties of pressure, temperature, and density used in the optimization process consist of 335 data points from temperature 283–386 K and pressure 1.30–34.6 MPa. Meanwhile, the available caloric data has a narrower range, namely temperature in range of 300 K to 350 K and pressure in range of 0.1 MPa to 10 MPa.

5.1 Visualization and Evaluation

The data uncertainty of Chen et al. [8] at 0.5% requires the minimum target deviation from this equation at 0.5%. The distribution of the ideal gas isobaric specific heat deviation concerning the Akasaka and Lemmon equation [6] and experimental data over the entire range appears in Figure 3. The difference in value from both EOS is less than 0.5%.

Deviation of the data from Akasaka and Lemmon [6] increases in the temperature range of 300 K because this range of the data from Chen et al. [8] was optimized using more weighting factor values. Figure 4 shows that the comparison concerning the data of Chen et al. [8] results in an average absolute deviation (AAD) of 0.48%, a standard deviation (STD) of 0.25%, and a maximum absolute deviation (MAX) of 0.94%. This result is already in the range of experimental data uncertainty.

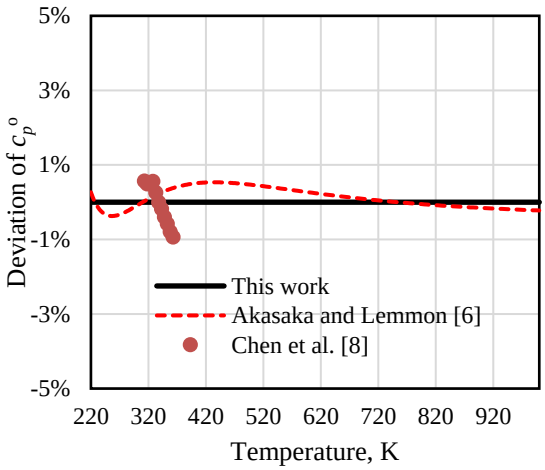

Figure 3. Deviation of the ideal gas specific heat.

There are five sources of experimental data used with temperature range of 233–376 K. The deviation of the vapor pressure from the new EOS to experimental data and artificial models can be seen in Figure 4.

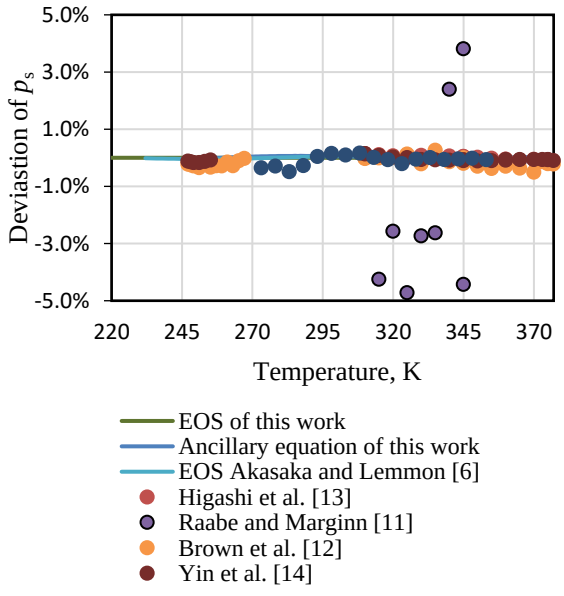

Figure 4. Deviation of the vapor pressures.

In the temperature range of 310–376 K, there are data set from Higashi et al. [13], which has an AAD of 0.070%, a MAX of 0.15%, and an STD of 0.033%. At a temperature range of 233–372 K, data sets from Brown et al. [12] were used, which have an AAD of 0.14%, a MAX of 0.85%, and an STD of 0.17%. At a temperature range of 263–353 K, data sets from Raabe and Marginn [11] were used. These data sets have an AAD of 4.4%, a MAX of 8.7%, and an STD of 2.1%.

Two recent data sets were obtained from Yin et al. [18], which have a temperature range from 253 to 376 K and have an AAD of 0.091%, a MAX of 0.17%, and an STD of 0.040%, and the data set of Yang et al. [15], which has a temperature range from 273 to 353 K and has an AAD of 0.14%, a MAX of 0.49%, and an STD of 0.14%.

Two data sets from Higashi and Sakoda [9] and Raabe and Marginn [11] fitted are the density at saturated liquid and vapor states. The amount of data available for saturated density is very scarce. Density deviations from the new EOS for the saturated-liquid and vapor states concerning experimental and derived property data are shown in Figures 5 and 6, respectively. For saturated liquid density data of Higashi and Sakoda [9], it results in an AAD of 0.56% with an STD of 0.23% and a MAX of 1.0%. Similar to the data for saturated steam, the data from Raabe and Marginn [16] yield a much higher deviation because the data are resulted from molecular modeling. These data produce an AAD of 3.1% with an STD of 1.1% and a MAX of 4.4%.

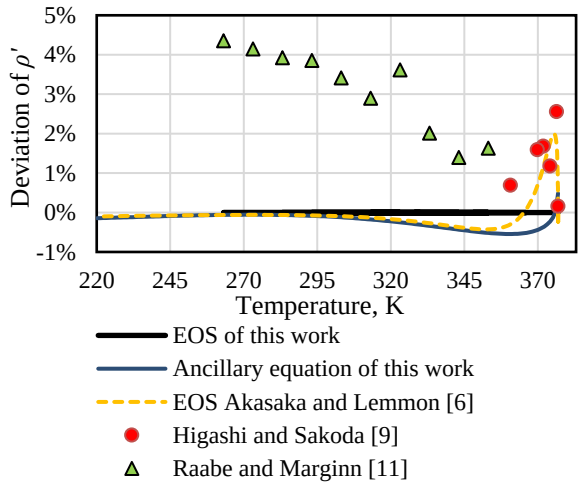

Figure 5. Deviation of saturated liquid density.

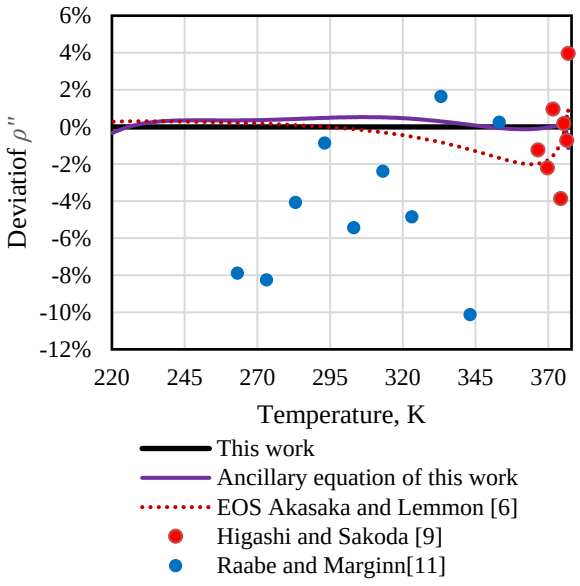

Figure 6. Deviation of the saturated vapor density.

For the saturated vapor density, data from Higashi and Sakoda [9] recorded an AAD of 1.3% with an STD of 0.97% and a MAX of 3.0%. Meanwhile, the data owned by Raabe and Marginn [11] performed AAD of 4.3% with an STD of 2.8% and a MAX of 8.7%.

In the temperature range of 328–386 K, there are data from Higashi et al. [13] having an AAD of 0.41%, a MAX of 1.1%, and an STD of 0.33%. On the other hand, at temperatures of 283–386 K, data from Brown et al. [12] have an AAD of 0.027%, a MAX of 0.35%, and an STD of 0.045%.

Figures 7 and 8 show the density deviation from the EOS concerning temperature and pressure, respectively. Experimental data on thermodynamic properties of pressure, temperature, and liquid density used in the optimization process consist of 269 data points from a temperature of 253–430 K and pressure of 0.110–6.86 MPa.

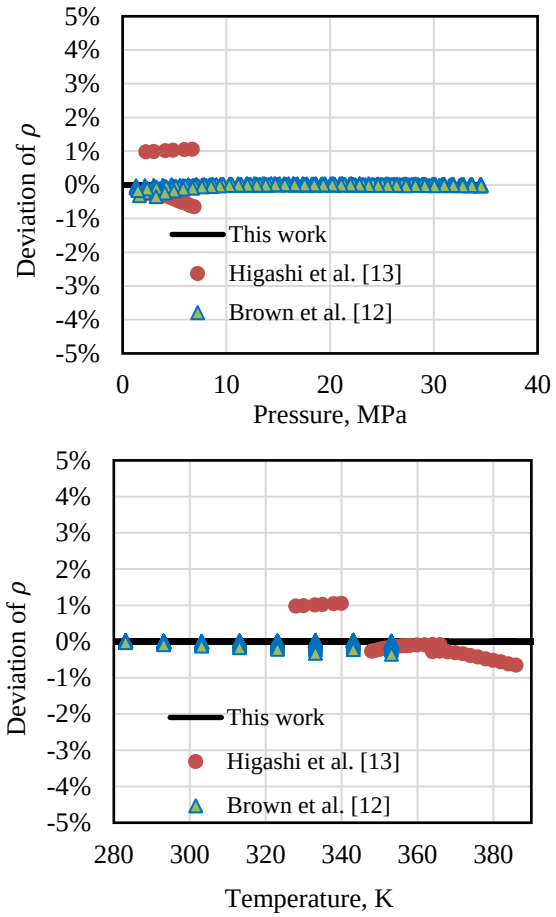

Figure 7. Deviation of the liquid density.

In the temperature range of 330 K to 430 K, the data from Higashi et al. [15] has an AAD of 0.55%, a MAX of 1.3%, and an STD of 0.35%. Meanwhile, data set from Brown et al. [17] for a temperature of 278–368 K has an AAD of 0.67%, a MAX of 2.8%, and an STD of 0.51%. The latest and most recent data set taken from Yin et al. [14] has a temperature range from 253 to 368 K and has an AAD of 0.25%, a MAX of 0.85%, and an STD of 0.21%.

The process of fitting the caloric properties of the fluid in the development of EOS is essential to get a good result of other properties such as internal energy, enthalpy, and entropy. Since the refrigerant of this study is relatively new, it is not widely applied. Only a set of experimental data is available. It is the isochoric heat data set reported by Sheng et al. [7]. and has 64 data points with a temperature range of 299–351 K. All these data are in the liquid phase. After comparing with the data calculated from the EOS of this work, it performs an AAD is 1.7% with an STD of 0.79% and a MAX of 3.3%. The deviation distribution appears in Figure 9.

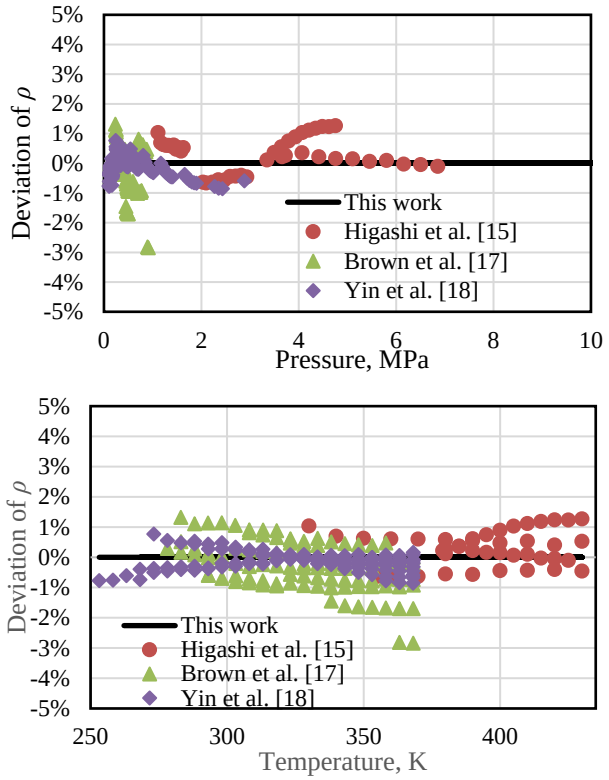

Figure 8. Deviation of the vapor density in the single phase.

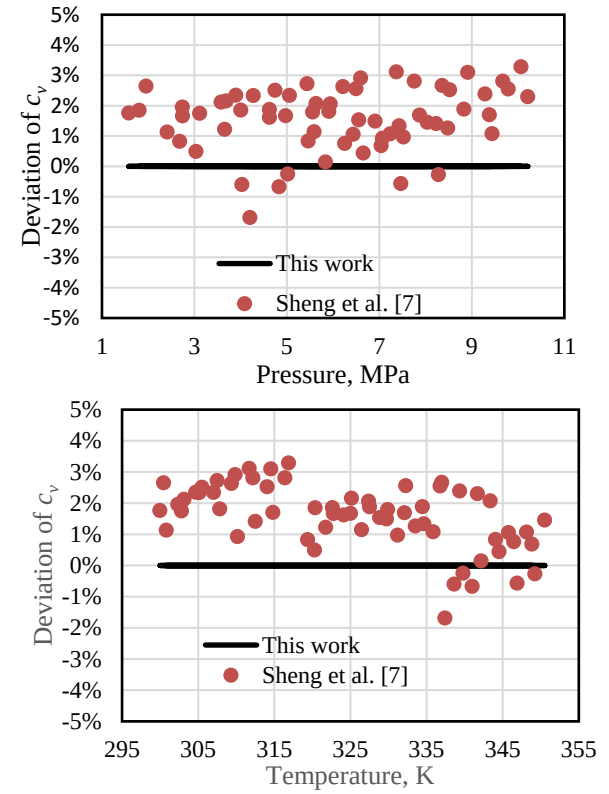

Figure 9. Deviation of the isochoric specific heat in the single phase.

The speed of sound data set available in the gas phase consists of 92 data points in the temperature range 313–363 K, which were reported by Chen et al. [8]. Compared to other property data, the speed of sound data has the highest accuracy. Chen et al. [8] claimed that the experimental data have an uncertainty of up to 0.018%. Because of its accuracy, higher weighting factors were given to the speed of sound data. The deviation of the experimental data concerning the data calculated from this work can be seen in Figure 10. This data set can be represented by the EOS with an AAD of 0.33%, an STD of 0.23%, and a MAX of 0.97%.

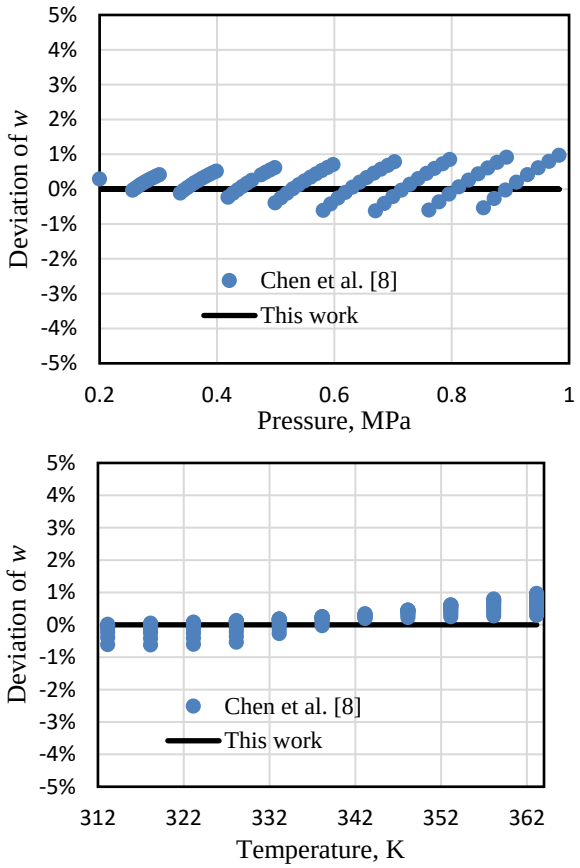

Figure 10. Deviation of the speed of sound in the single phase.

5.2 Thermodynamic Consistencies

It is not sufficient just to evaluate the performance of the equation by comparing experimental data and calculated data, especially if the experimental data available is limited. The extrapolation behavior of the equations in this study was assessed from the plot of pressure and specific volume curves on isothermal lines, plots of caloric properties curves (isochoric specific heat, isobaric specific heat, and speed of sound) on isobaric lines, ideal curves (inverse Joule-Thomson curve, Boyle curve, and Joule inverse curve), and the second and third virial coefficients.

Extrapolation curves for pressure, specific volume, and temperature can be seen in Figure 11. The curves were plotted within a temperature range of 220–1000 K and a pressure range of 0.025–1000 MPa. In single-phase, the resulting curve has a reasonable shape without any intersecting isotherm line from low to high temperatures. In the saturation state, the saturated lines have a proper shape; the lines rise at the saturated-liquid state and flatten out at the critical point and two-phase, then decrease at the saturated vapor condition. Under two-phase conditions, all isothermal lines are at the same pressure.

Next, the extrapolation curve for the caloric properties is evaluated. The extrapolation curve for caloric properties was plotted within the temperature range of 220–750 K and the pressure range of 0.025–100 MPa. The first caloric property to be discussed is isochoric specific heat. The isochoric-specific heat curve requires special observations because the shape of this curve is very sensitive to the changes in the

equation term, and because only experimental data available for specific heat is isochoric-specific heat data. The isochoric-specific heat extrapolation curve can be seen in Figure 12. In general, isochoric-specific heat curves have a reasonable shape. In the liquid state, the isobaric lines have an upward trend as the temperature increases, then increases drastically near the critical point then decreases, and then rises again at very high temperatures. In the liquid phase at low temperatures, there are few waves on the curve and the isobaric lines appear to coincide. The curve in this low-temperature range can be seen in Figure 13. Even so, the trend line remains upward on all the isobaric lines. There is no line intersecting each other.

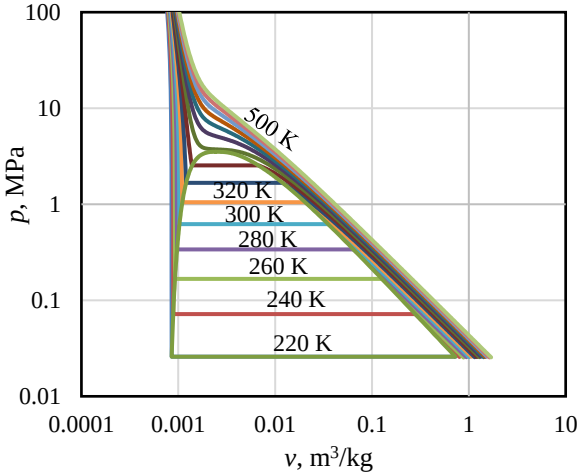

Figure 11. PVT Extrapolation of the new EOS.

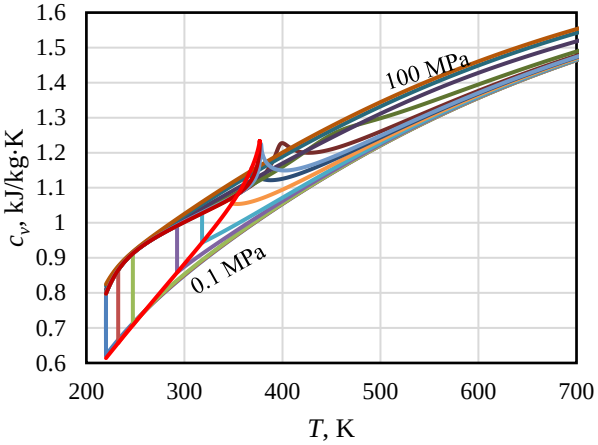

Figure 12. Isochoric heat extrapolation of the new EOS.

The experimental data available for isochoric heat are only within the temperature range of 299–351 K and pressure range of 1.50–10.2 MPa. Therefore, a new set of data in the temperature and pressure ranges as shown in Figure 13 is needed to ensure that the shape of the extrapolation curve is closer to the actual conditions.

Figures 13 and 14 show extrapolation curves for isobaric-specific heat and speed of sound, respectively. The extrapolation curves for these two thermodynamic properties already have a reasonable shape within the temperature and pressure range. In an isobaric heat curve, the trend is like that in an isochoric-specific heat curve. As the isobaric line approaches the critical point, the curve will rise sharply, decrease rapidly to a specific value, and then ramp up with increasing temperature. As for the speed-of-sound curves, isobaric lines in the critical region follow a different trend, decreasing with increasing temperature in the liquid phase and rising with increasing temperature in the gas phase. The minimum value occurs at the critical point.

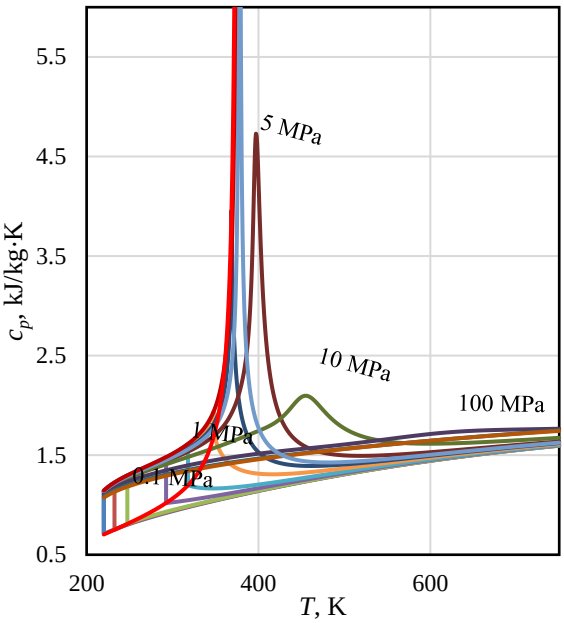

Figure 13. Isobaric heat extrapolation of the new EOS.

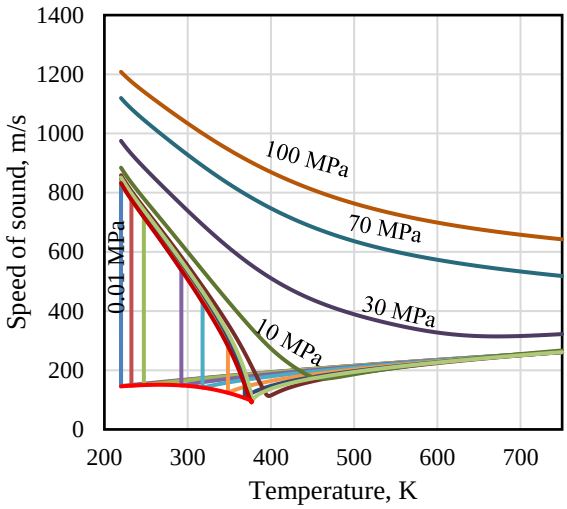

Figure 14. Speed of sound extrapolation of the new EOS.

Ideal curves do not provide numerical information, but rational behaviors can represent a good extrapolation ability of the equation. Figure 15 shows the curve comparison from the EOS of this work and Akasaka and Lemmon [6]. In general, the four curves have the same trend, large values at low temperatures, and then their value drops drastically at high temperatures by turning downwards to form an asymptote line. For the ideal curves of the Akasaka and Lemmon EOS, don't follow this trend at high temperatures. On the other hand, the Boyle curve, the Joule inversion curve, and the Joule-Thomson curve have good agreement between the EOS of this study and Akasaka and Lemmon.

The last parameter that needs to be evaluated to determine the extrapolation ability of the equation is the second and third virial coefficients. The appropriate shape of virial coefficient curves can represent a good equation extrapolation ability. In general, the shape of a good virial coefficient curve is going upward drastically at low temperatures, then form asymptotes towards zero pressure at

very high temperatures. The second and third virial coefficient curves calculated respectively are shown in Figures 16 and 17. In the second virial coefficient graph, the curve obtained from the EOS in this work coincides with the curve from the experimental data (Yin et al. [14] and Chen et al. [8]) as well as the curves obtained from Akasaka and Lemmon [8]. The third virial coefficients obtained from this work do not coincide with the data compared (Yin et al. [14], and Akasaka and Lemmon [6]), but they have the same trend.

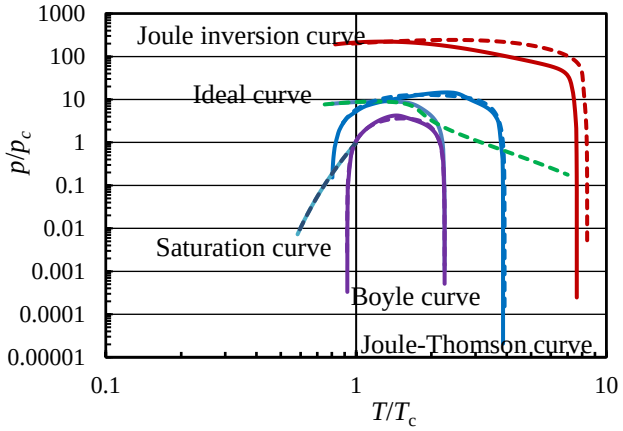

Figure 15. Ideal curves of the new EOS with solid curves of this work, dashed curves of Akasaka and Lemmon EOS.

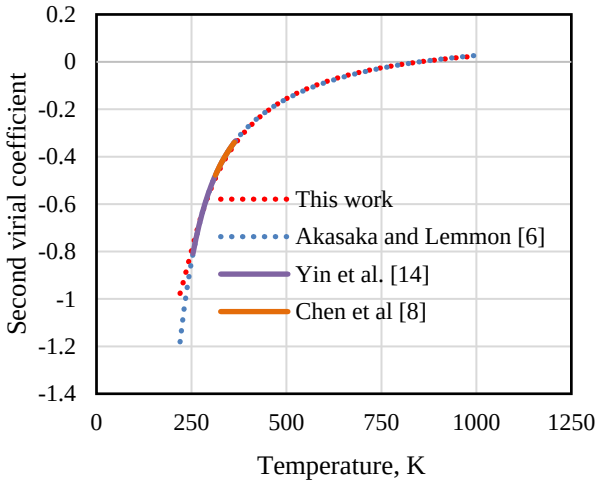

Figure 16. Behavior of second virial coefficients from the new EOS.

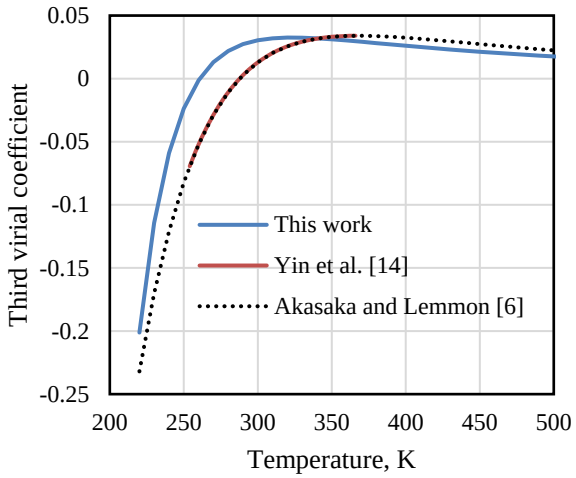

Figure 17. Behavior of third virial coefficients from the new EOS.

5.3 Statistical Comparison

To further assess the quality of the new EOS from this work, a detailed statistical evaluation between EOS of this work and other existing EOS is given. Better statistics mean having smaller values for each parameter (AAD, STD, and MAX), although in this evaluation, the STD results are not used much because the results of the AAD and the MAX are sufficient for comparison. The new EOS compared to is the Akasaka and Lemmon EOS [6], because it is the latest existing EOS.

The first evaluation that will be carried out is density in single phase. A comparison of statistics can be seen in Table 5. In the liquid phase, the EOS in this study has a better AAD than the data of Di Nicola et al. [16] but worse than Higashi and Sakoda [9]. The opposite condition applies to the MAX data. This result happens because in both data sets, there are data points that are near saturation conditions, so that in these areas, it is difficult to get a good deviation. In the gas phase, the deviation is generally better on Higashi and Sakoda [14] and Yin et al. [14], but worse on Di Nicola et al. [16]. This happens because the fitting process is intended to be closer to the data of Yin et al. [14], which used fluid with higher purity for the experiment.

Comparison of the liquid and saturated density can be seen in Tables 5 and 6, respectively. In general, these two properties have the same statistical comparison. The statistics for Raabe and Marginn data [11] are better than the Akasaka and Lemmon [6] but worse for Higashi and Sakoda [9]. It happened because the data of Higashi and Sakoda [9] are very close to the critical point causing difficulty in the fitting process. This difficulty is due to the structural form of the equation excluding the Gaussian-Bell form. However, the resulting deviation is quite close compared to the equation of Akasaka and Lemmon [6].

Statistical comparison for caloric and ideal properties can be seen in 7. All data on caloric and ideal properties from the equations in this study have better statistics than the Akasaka and Lemmon [6].

6. Conclusion

The new EOS of R-1243zf has the functional form of Helmholtz-free energy. The optimization was conducted using a genetic algorithm and weighted-least squares regression. The EOS can provide accurate results of the thermodynamic properties when compared to the experimental data. In general, the accuracy of the proposed EOS is better than the Akasaka and Lemmon EOS, except for the saturation states. Evaluation for the extrapolation ability consists of thermodynamic properties at temperatures outside the experimental data, ideal curves, and the second and third virial coefficients. Based on the evaluation, this equation has a good extrapolation ability judged by the shape of the curves under the theories of thermodynamics. Further evaluation is needed for the isochoric-specific heat curve due to the lack of available experimental data.

The proposed EOS consists of two parts: the ideal and residual parts. Ancillary equations for properties on saturated condition were also developed to assist the optimization process and to calculate the thermodynamic properties from the EOS. The ideal part was developed with the ideal isobaric specific heat data. The properties derived from ideal part compared to the experimental data yielded an AAD of 0.48%, an STD of 0.25%, and a MAX of 0.94%. The residual part was developed with multi-property input data. In saturation state, there are three properties used, saturated

Table 5. Statistical comparison results of EOS.

Prop.	Data Source	EOS*	Points	Phase	AAD (%)	STD (%)	MAX (%)
PVT	Di Nicola et al. [16]	New	302	Liquid	0.0270	0.0450	0.350
		Exist			0.0330	0.0240	0.0910
PVT	Higashi & Sakoda [9]	New	33	Liquid	0.411	0.340	1.06
		Exist			0.253	0.390	1.12
PVT	Di Nicola et al. [16]	New	99	Gas	0.667	0.510	2.77
		Exist			0.592	0.480	2.35
PVT	Higashi & Sakoda [9]	New	42	Gas	0.548	0.350	1.28
		Exist			0.731	0.520	1.78
PVT	Yin et al. [14]	New	128	Gas	0.245	0.211	0.850
		Exist			0.347	0.195	1.01
p_s	Raabe & Marginn [11]	New	10	-	4.38	2.05	8,69
		Exist			4.40	2.04	8,70
p_s	Brown et al. [12]	New	83	-	0.138	0.168	0.851
		Exist			0.150	0.167	0.834
p_s	Higashi et al. [13]	New	20	-	0.0700	0.0330	0.147
		Exist			0.0260	0.0210	0.0860
p_s	Yin et al. [14]	New	26	-	0.0910	0.0400	0.170
		Exist			0.108	0.0370	0.165
p_s	Yang et al. [15]	New	17	-	0.141	0.135	0.490
		Exist			0.155	0.138	0.504
ρ'	Raabe & Marginn [11]	New	10	-	3.12	1.03	4.35
		Exist			3.29	0.910	4.41
ρ'	Higashi & Sakoda [9]	New	6	-	1.31	0.760	2.56
		Exist			0.790	0.210	0.980
ρ''	Raabe & Marginn [11]	New	10	-	4.58	3.20	10.1
		Exist			4.65	2.79	8.80
ρ''	Higashi & Sakoda [9]	New	7	-	1.88	1.41	3.97
		Exist			1.32	0.960	3.03
c_p^0	Chen et al. [8]	New	11	Gas	0.478	0.252	0.936
		Exist			0.597	0.369	1.32
c_v	Sheng et al. [7]	New	64	Liquid	1.71	0.792	3.29
		Exist			2.35	0.719	3.82
w	Chen et al. [8]	New	92	Gas	0.330	0.234	0.969
		Exist			0.441	0.307	1.29

*Exist is the EOS developed by Akasaka and Lemmon [6]; New is the EOS from this study.

pressure, which has an AAD of 0.96%, an STD of 0.49%, and a MAX of 2.1%; saturated liquid density which has an AAD of 2.2%, an STD of 0.89%, and a MAX of 3.5%; and the saturated vapor density which has an AAD of 3.2%, an STD of 2.3%, and a MAX of 7.1%. In single-phase, for the liquid density data, this equation has an AAD of 0.22%, an STD of 0.19%, and a MAX of 0.71%. For gas density data, this equation has an AAD of 0.49%, an STD of 0.36%, and a MAX of 1.6%. The final data is from the caloric properties, which consist of isochoric specific heat, which has an AAD of 1.7%, an STD of 0.79%, and a MAX of 3.3%; and the speed of sound data which has an AAD of 0.33%, an STD of 0.23%, and a MAX of 0.97%.

Ancillary equations were developed for saturated pressure, saturated liquid density and saturated vapor density. For saturated pressure, the developed ancillary equation has an AAD of 0.96%, an STD of 0.47%, and a MAX of 2.1%. For the saturated liquid density, the ancillary equation in this work has an AAD of 1.9%, an STD of 0.65%, and a MAX of 2.7%; and the saturated vapor density which has an AAD of 2.8%, an STD of 1.9%, and a MAX of 5.8%.

Nomenclature

Symbols

A	Helmholtz free energy [kJ·kg^{-1}]
AAD	Average absolute deviation
B	Second virial coefficient [dm^3·mol^{-1}]
b	Numerical coefficient
C	Third virial coefficient [dm^6·mol^{-2}]
c	Specific heat capacity [kJ·kg^{-1}·K^{-1}]
d	Numerical constant
E	Numerical coefficient
F	Numerical coefficient
G	Numerical coefficient
M	Molar mass [kg·kmol^{-1}]
MAX	Maximum deviation
N	Numerical Coefficient
R	Gas constant [kJ·kg^{-1}·K^{-1}]
$\bar{R}$	Universal gas constant [J·mol^{-1}·K^{-1}]
s	Specific entropy [kJ·kg^{-1}·K^{-1}]
STD	Standard deviation
T	Temperature [K]
t	numerical constant
u	Internal energy [kJ·kg^{-1}]
p	Pressure [MPa]
PVT	Pressure Volume Temperature

W	Weighting factor
w	Speed of sound [$m \cdot s^{-1}$]
χ	Sum of weighted least square
Greek Letters	
α	Reduced Helmholtz free energy, A/RT
δ	Reduced density, ρ/ρ_c
θ	Numerical constant
ρ	Density [$kg \cdot m^{-3}$]
τ	Inverse reduced temperature, T_c/T
Subscript	
c	Critical parameter
cal	Calculated value
data	Input data value
i	Serial number of term
p	Process at constant pressure
s	Saturation
tp	Triple point
v	Process at constant volume
Superscripts	
o	Ideal part
r	Residual part
‘	Saturated-liquid state
“	Saturated-vapor state

References:

[1] UN, *Amendment to the Montreal Protocol on Substances that Deplete the Ozone Layer*, New York: United Nations, 2016.

[2] B. Gil, J. J. Kasperski, "Efficiency Evaluation of the Ejector Cooling Cycle using a New Generation of HFO/HCFO Refrigerant as a R134a Replacement," *Energies*, 11(8), 2136, 2018, doi: 10.3390/ en11082136.

[3] JSRAE, "Risk Assessment of Mildly Flammable," JSRAE, Tokyo, 2015.

[4] N. A. Lai, "Thermodynamic Properties of HFO–1243zf and Their Application in Study on a Refrigeration Cycle," *Applied Thermal Engineering*, 70(1), 1–6, 2014, doi: 10.1016/j.app lthermaleng.2014.04.042.

[5] R. Akasaka, "Recent Trends in the Development of Helmholtz Energy Equations of State and Their Application to 3,3,3-Trifluoroprop-1-ene (R-1243zf)," *Science and Technology for the Built Environment*, 22(8), 1136–1144, 2016, doi: 10.1080 /23744731.2016.1208000.

[6] R. Akasaka, E. W. Lemmon, "Fundamental Equations of State for cis-1,3,3,3- Tetrafluoro propene [R-1234ze(Z)] and 3,3,3-Trifluoropropene (R-1243zf)," *Journal of Chemical and Engineering Data*, 64(11), 4679–4691, 2019, doi: 10.1021/ acs.jced.9b00007.

[7] B. Sheng, Z. Li, W. Liu, X. Chen, Y. Zhao, X. Dong, H. Yan, J. Shen, M. M. Gong, "The Isochoric Special Heat Capacity for 3,3,3-Trifluoroprop-1-ene (R1243zf) at Temperatures from (299 to 351) K and Pressures up to 11 MPa," *The Journal of Chemical Thermodynamics*, 153, 106319–106324, 2021, doi: 10.1016/j.jct.2020.106319.

[8] H. Chen, K. Zhang, Z. Yang, Y. Y. Duan, "Experimental Speed of Sound for 3,3,3-Trifluoropropene (R-1243zf) in Gaseous Phase Measured with Cylindrical Resonator," *Journal of Chemical and Engineering Data*, 66(5), 2256–2263, 2021, doi: 10.1021/acs.jced.1c00098.

[9] Y. Higashi, N. Sakoda, "Measurements of PvT Properties, Saturated Densities, and Critical Parameters for 3,3,3-Trifluoropropene (HFO1243zf)," *Journal of Chemical and Engineering Data*, 63(10), 3818–3822, 2018, doi: 10.1021/acs.jced.8b00452.

[10] E. Tiesinga, P. J. Mohr, D. B. Newell, B. N. Taylor, "CODATA Recommended Values of the Fundamental Physical Constants: 2018," *Journal of Physical and Chemical Reference Data*, 50(3), 033105, 2021, doi: 10.1063/5.0064853.

[11] G. Raabe, E. J. Maginn, "A Force Field for 3,3,3-Fluoro-1-propenes, Including HFO-1234yf," *The Journal of Physical Chemistry B*, 114(31), 10133–10142, 2010, doi: 10.1021/jp102534z.

[12] J. S. Brown, G. di Nicola, L. Fedele, S. Bobbo, C. Zilio, "Saturated Pressure Measurements of 3,3,3-Trifluoroprop-1-ene (R1243zf) for Reduced Temperatures Ranging from 0.62 to 0.98," *Fluid Phase Equilibria*, 351, 48–52, 2013, doi: 10.1016/ j.fluid.2012.09.036.

[13] Y. Higashi, N. Sakoda, M. A. Islam, Y. Takata, S. Koyama, R. Akasaka, "Measurements of Saturation Pressures for Trifluoroethene (R1123) and 3,3,3-Trifluoropropene (R1243zf)," *Journal of Chemical and Engineering Data*, 63(2), 417–421, 2018, doi: 0.1021/acs.jced.7b00818.

[14] J. Yin, J. Ke, G. Zhao, S. Ma, "Saturated Vapor Pressure and Gaseous pvT Property Measurements for 3,3,3-Trifluoroprop-1-ene (R1243zf)," *Int. J. of Refrigeration*, 117, 175–180, 2020, doi: 10.1016/ j.ijrefrig.2020.04.021.

[15] Z. Yang, A. Valtz, C. Coquelet, J. Wu, J. Lu, "Experimental Measurement and Modelling of Vapor-Liquid Equilibrium for 3,3,3-Trifluoro propene (R1243zf) and trans-1,3,3,3-Tetrafluoro propene (R1234ze(E)) Binary System," *Int. J. of Refrigeration*, 120, 137–149, 2020, doi: 10.1016/ j.ijrefrig.2020.08.016.

[16] G. di Nicola, J. S. Brown, L. Fedele, M. Securo, S. Bobbo, C. Zilio, "Subcooled Liquid Density Measurements and PvT Measurements in the Vapor phase for 3,3,3-Trifluoroprop-1-ene (R1243zf)," *Int. J. of Refrigeration*, 36(8), 2209–2215, 2013, doi: 10.1016/j.ijrefrig.2013.08.004.

[17] K. G. Joback, R. C. Reid, "Estimation of Pure-Component Properties from Group-Contributions," *Chemical Engineering Communications*, 57(1–6), 233–243, 1987, doi: 10.1080/00986448708960487.

[18] R. Span, Multiparameter Equations of State: An Accurate Source of Thermodynamic Property Data,

Berlin: Springer, 2000, doi: 10.1007/978-3-662-04092-8.

[19] W. Wagner, A. Pruß, "The IAPWS Formulation 1995 for the Thermodynamic Properties of Ordinary Water Substance for General and Scientific Use," *Journal of Physical and Chemical Reference Data,* 31(2), 387–535, 2022, doi: 10.1063 /1.1461829.

[20] I. M. Astina, G. Budiarso, R. Horrison, "New Helmholtz Equation of State for HFO-1234ze(E) with Comprehensive Assessment," *Fluid Phase Equilibria,* 531, 112921, 2021, doi: 10.1016/j.fluid .2020.112921.

[23] E. W. Lemmon, R. T. Jacobsen, "A New Functional Form and New Fitting Techniques for Equations of State with Application to Pentafluoroethane (HFC-125)," *Journal of Physical and Chemical Reference Data,* 34(1), 69–108, 2004, doi: 10.1063/1.179 7813.

[21] G. Budiarso, I. M. Astina, "Development of Helmholtz Equation of State for Thermodynamic Properties of R-1233zd(E)," *Int. Journal of Scientific Research in Science and Technology,* 9(3), 765–776, 2022, doi: 10.32628/IJSRST2293 148.

[22] I. M. Astina, H. Sato, "A Rapid Genetic Optimization Technique for Rational Thermodynamic Modeling Having Reliable Third Virial Coefficient," in *15th Symposium on Thermophysical Properties*, Boulder, 2003.